Thermoelectric transport in periodic one-dimensional stacks of InAs/GaAs quantum dots

V. M. Fomin[1,*] and P. Kratzer[2,†]
[1]*Institute for Integrative Nanosciences, IFW Dresden, Helmholtzstr. 20, D-01069 Dresden, Germany*
[2]*Fakultät für Physik and Center for Nanointegration (CeNIDE), Universität Duisburg-Essen, Lotharstr. 1, D-47048 Duisburg, Germany*
(Received 22 January 2010; revised manuscript received 2 July 2010; published 27 July 2010)

We investigate the effect of the narrow electronic minibands of periodic one-dimensional stacks of disk-shaped InAs quantum dots (QDs) in GaAs on their electronic transport characteristics by employing an empirical tight-binding calculation and a continuum model of the electronic structure. Our model includes both the minibands and the continuum of the host conduction band. The rate of the electron-acoustic-phonon scattering is found using Boltzmann's semiclassical transport theory. The electric conductivity, the Seebeck coefficient and the thermoelectric figure-of-merit for *n*-doped QD arrays are then analyzed as a function of the donor concentration and temperature. For QDs several nanometers in height, the figure-of-merit at temperatures below 100 K as a function of doping is richly structured, reflecting the miniband electron energy spectrum of a QD stack. Certain windows of concentration are revealed, where QD arrays display a geometry-controlled enhanced efficiency as thermoelectric converters. For optimizing the peak values of the figure-of-merit attainable for donor concentrations within the experimentally accessible range, a very thin spacer layer between the QDs ($\lesssim 5$ nm) is found to be most suitable. Assuming that the lattice thermal conductivity can be reduced below 0.5 W/(m K), a figure-of-merit larger than 2 appears within reach.

DOI: 10.1103/PhysRevB.82.045318 PACS number(s): 73.21.La, 73.22.−f, 72.20.Pa

I. INTRODUCTION

The use of nanostructured materials as a way to enhance thermoelectric properties has acquired increasing interest in recent years. In contrast to the bulk materials conventionally used in thermoelectrics, which are often difficult to synthesize in a controlled way due to their complex crystal structure, the technology for fabricating nanocomposites of standard semiconductors, such as Si, Ge, InAs, or GaAs, has matured. Hence, such structures offer new possibilities for the design of thermoelectric devices with an improved efficiency by exploiting the quantum confinement of electrons and phonons on the nanoscale. Proposals of quantum-confined structures (quantum wells and quantum wires) with the goal of obtaining a high figure-of-merit from nonconventional thermoelectric materials date back to 1993.[1] Nanostructuring of materials has proven particularly helpful in reducing the thermal conductivity (that enters in the denominator in the thermoelectric figure-of-merit *ZT*). This is mostly due to the interfaces in a composite material acting as thermal barriers.

Here, we are addressing the question how semiconductor nanostructures could be used to enhance the *electronic transport coefficients* that enter the figure-of-merit. From thermodynamic arguments, it has been shown that the thermoelectric efficiency is maximum if the carrier transport is isentropic.[2] A narrow distribution of the energy of the carriers participating in the transport process was shown to be crucial for achieving this goal.[3] In particular, tailoring the electronic density of states in the vicinity of the Fermi level can increase the thermopower. Motivated by these considerations, quantum dot (QD) crystalline arrays (superlattices) embedded in a wide-gap host material appear to be promising: The narrow features in the density of states due to quasiconfined electronic states could considerably modify the thermoelectric properties compared to the host material. It was shown recently that the electron thermoelectric tunneling coefficients of a single QD weakly coupled to two electron reservoirs can be significantly affected by its electron energy spectrum.[4] However, as indicated in Ref. 5, "quantum confinement effects, if present, would be limited to the QDs themselves and this would not explain why the *ZT* of the total composite is enhanced."

For practically important one-dimensional (1D) (see Ref. 6), two-dimensional (2D), and three-dimensional (3D) (see Refs. 7 and 8) QD crystalline arrays (superlattices), strong coupling between QDs leads to formation of extended minibands instead of localized QD states. Extended states in minibands can be formed even in the presence of disorder as long as the bandwidth due to wave function overlap exceeds the total broadening, which is mainly due to the disorder (inhomogeneous broadening). Miniband formation in a *p*-type superlattice of Ge QDs in Si is theoretically shown to provide enhancement of the thermoelectric figure-of-merit.[8] Feasibility of the improvement of the thermoelectric characteristics has been experimentally studied in PbSeTe-based QD superlattice structures; the quantitative data on the achievable values of *ZT* are still an open issue (cp. Ref. 9 with Ref. 10). Of special importance is the possibility to achieve a simultaneous increase in the thermoelectric power factor σS^2 (where σ is the electric conductivity and S is the Seebeck coefficient) and a decrease in the thermal conductivity in the same nanocomposite sample.[11] Recently, enhanced values of thermoelectric figure-of-merit were achieved in nanostructured *p*-type BiSbTe[12] and SiGe[13] alloys. Control of thermal conductivity down to the sub-1 W m^{-1} K^{-1} range at the nanoscale via individual phonon scattering barriers has been achieved in multilayered Ge/Si QD arrays with as little as 5 barriers.[14]

Recent theoretical efforts are aimed at clarification of mechanisms underlying the enhancement of the thermoelectric efficiency for nanocomposites. Transport properties of QD crystalline arrays studied with dynamical mean-field

theory[15] indicate that the material is metallic with a large thermopower. The calculation based on a self-consistent solution of the Schrödinger and Poisson equations in Ref. 16 suggests that the incorporation of InAs QD chains into a GaAs matrix can increase its thermoelectric power factor by a factor of 3. An enhancement of the thermoelectric power factor in InGaAlAs semiconductors with metallic nanoinclusions of ErAs at high doping concentrations has been analyzed within the partial-wave technique and the relaxation time approximation.[17,18]

Moreover, experimental progress in the quantitative characterization of QDs as elements for thermoelectric devices has been made by evaluating the temperature-dependent thermopower in GaAs/AlGaAs QDs[19] and a temperature differential across a QD.[20,21] Another technique, based on the detection of magnetoconductance fluctuations, provides experimental evidence for hybridization of electron wave functions in $Ga_{0.25}In_{0.75}As/InP$ QD arrays.[22] It has been shown theoretically, that tunneling through a single QD with well-separated resonant energies results in a linear material-independent behavior of the Seebeck coefficient for small deviations of the chemical potential from a resonant energy.[23]

The present paper addresses the effect of the miniband energy spectrum on the electronic transport characteristics in a periodic 1D stack of disk-shaped InAs QDs in GaAs, which can be produced by self-organized anisotropic strain engineering.[24] This method has been successfully applied to fabricate InGaAs/GaAs QD chains[25,26] and seeded 3D arrays of Ge/Si[27] and InGaAs/GaAs[28] QDs.

The paper is organized as follows. In Sec. II, we outline the theoretical approach to calculate the electronic transport in a periodic 1D stack of QDs. The atomistic and continuum models of electron minibands used for QD stacks are described in Secs. III and IV, respectively. The scattering rate due to the deformation interaction of electrons with acoustic phonons is calculated in Sec. V. (The details of the evaluation of the scattering rate are presented in Appendix.) On that basis, the relaxation time is found as a solution of the Boltzmann transport equation in Sec. VI. Populating the minibands by *n*-type doping, as discussed in Sec. VII, turns out to be crucial for exploiting the advantages of the InAs/GaAs structures. We analyze the behavior of transport coefficients as a function of the donor concentration in Sec. VIII. Conclusions on the geometry-controlled enhancement of thermoelectric efficiency of stacks of QDs are drawn in Sec. IX.

II. OUTLINE OF THE THEORETICAL APPROACH

We consider a stack of semiconductor QDs embedded in a host material with larger band gap. For simplicity, flat disk-shaped QDs with radius R are assumed. The spacer layer between the QDs is taken to be sufficiently thin to allow for coherent tunneling, thus leading to the formation of minibands. Our goal is the calculation of the thermoelectric coefficients in cross-plane geometry, with the electric current flowing along the QD stack. Contributions to the current both from the electronic states bound in the QD, broadened into minibands, and from the continuum of electronic states of the host material are taken into account. Electronic transport is treated at the semiclassical level using the Boltzmann equation solved within the relaxation time approximation. Following Ashcroft and Mermin,[29] the transport coefficients are computed from the moments $\mathcal{L}^{(\alpha)}$ of the distribution function

$$\mathcal{L}^{(\alpha)} = \sum_J \frac{2}{\mathcal{A}} \int_0^{\pi/d_z} \frac{dk_z}{2\pi} \left(-\frac{\partial f_0}{\partial \varepsilon} \right) \tau_{\parallel,J}(k_z) v_{z,J}^2(k_z) (\varepsilon_J(k_z) - \mu)^\alpha + \frac{2}{(2\pi)^3} \int d^3k \left(-\frac{\partial f_0}{\partial \varepsilon} \right) \tau_\parallel^{(1)}(\varepsilon) v_z^2(\mathbf{k}) (\varepsilon(\mathbf{k}) - \mu)^\alpha. \quad (1)$$

Here, the first integral accounts for miniband transport, while the second integral accounts for transport in a band continuum, e.g., in the host conduction bands. The factor 2 in front of the integrals results from spin degeneracy, J numbers the minibands, and $\mathcal{A} = \pi R^2$ is the cross-sectional area of the stack. The αth moment is evaluated using the equilibrium Fermi distribution function at temperature T,

$$f_0(\varepsilon) = \left[\exp\left(\frac{\varepsilon - \mu}{k_B T} \right) + 1 \right]^{-1}.$$

Here, μ is the chemical potential of the electrons, which is determined from the nature and concentration of dopants (see Sec. VII). Each miniband J is characterized by its dispersion relation $\varepsilon_J(k_z)$, the resulting group velocity $v_{z,J}(k_z)$ and the relaxation time $\tau_{\parallel,J}(k_z)$. For the continuum states, the same quantities are denoted by functions of the three-dimensional wave vector $\mathbf{k}$ or the energy ε. The remainder of this paper is devoted to developing microscopic models for the miniband dispersion, and to calculating $\tau_{\parallel,J}(k_z)$ [see Eq. (16)] and $\tau_\parallel^{(1)}(\varepsilon)$ [see Eq. (19)] for deformation potential scattering due to acoustic phonons.

Once the $\mathcal{L}^{(\alpha)}$ are known, the electric conductivity

$$\sigma = e^2 \mathcal{L}^{(0)}, \quad (2)$$

the Seebeck coefficient

$$S = -\frac{1}{eT} \frac{\mathcal{L}^{(1)}}{\mathcal{L}^{(0)}}, \quad (3)$$

and the electronic heat conductivity

$$\kappa_e = \frac{1}{T} \left(\mathcal{L}^{(2)} - \frac{[\mathcal{L}^{(1)}]^2}{\mathcal{L}^{(0)}} \right) \quad (4)$$

can be calculated. The dimensionless figure of merit, which determines the power generation efficiency of a thermoelectric converter,[30] is defined as

$$ZT = \frac{\sigma S^2 T}{\kappa}, \quad (5)$$

where the thermal conductivity $\kappa = \kappa_e + \kappa_{ph}$ contains both electron (κ_e) and lattice (κ_{ph}) contributions.

III. ATOMISTIC MODEL OF QUANTUM DOT STACKS

It is interesting to investigate under which conditions QDs possess quasibound states suitable for thermoelectric trans-

TABLE I. Single-particle energy levels of electronlike states confined in the disk-shaped InAs quantum dots in GaAs matrix. All energies for the band minima (k_z=0) are measured from the valence band top of (strain-free) GaAs. The energy values in parentheses are the band widths.

d_z	18 L	22 L		26 L		
d_z, nm	5.14	6.26	6.27	7.39	7.39	7.41
a_z, nm	1.57(5L)	1.57(5L)	2.19(7L)	1.57(5L)	2.19(7L)	2.82(9L)
E_1, meV	1224 (60)	1227 (28)	1169 (26)	1226 (13)	1167 (12)	1131 (12)
E_2, meV	1314 (48)	1317 (19)	1266 (19)	1317 (11)	1265 (7)	1234 (8)
E_3, meV		1390 (49)	1373 (27)	1391 (25)	1372 (16)	1353 (11)

port, and how the energetic position and width of the minibands derived from these states depend on geometrical and materials parameters. To learn about these issues, we consider a specific materials system, InAs QDs embedded in a host of GaAs. We consider an infinitely repeated stack of disk-shaped quantum dots of radius R=5 nm. For the height of the InAs cylinders a_z and for the vertical stacking period d_z, values of 5 (also 7 and 9) and 18 (also 22 and 26) layers (L) of InAs or GaAs, respectively, have been chosen. For computational convenience, we employed a geometry that is periodic in all three dimensions. The period $d_x=d_y$ =20.91 nm in the xy plane has been chosen large enough such that any dispersion of the confined states along x and y is negligible (<1 meV). A 'wetting layer' of one monolayer of InAs has been included to model a realistic atomic structure as it results from self-assembling heteroepitaxy. The period d_z is determined by the following consideration: Given the total number of Ga and In atoms in the 3D unit cell, d_z corresponds to the estimated thickness a random-alloy film of $In_xGa_{1-x}As$ with the same net composition would assume, if biaxially strained to match the lattice constant of the GaAs substrate in the x and y directions. Within the, thus, determined 3D box, the positions of all atoms are elastically relaxed, using a classical interatomic potential of Tersoff type. The parameterization of this potential has been chosen to match all three elastic constants for both bulk GaAs and InAs.[31]

The atomic positions obtained after relaxation are input to an empirical tight-binding (ETB) calculation of the electronic structure. Elastically relaxed bond distances and bond angles enter into the tight-binding Hamiltonian via a parameterized distance dependence of the ETB matrix elements and via the bond-angle dependence of the Slater-Koster factors, respectively. We use an sp^3s^* ETB parameterization with both first and second-nearest-neighbor interactions and spin-orbit coupling.[32] For the offset between the valence bands of GaAs and InAs, a value of 0.054 eV was used.[33] Further details can be found in previous calculations using the same setup.[34,35] The isolated eigenvalues corresponding to confined electronic states within the band gap of the GaAs matrix are calculated iteratively, using the "folded-spectrum" method.[36,37] Along the z direction, periodic boundary conditions are employed using Bloch's theorem.

The InAs QDs display both shallow "holelike" states derived from the valence band, and more strongly bound "electronlike" states derived from the conduction band. Since we are interested in n-type conductivity, we discuss only the electronlike states. For the geometries studied, we usually find three bound states, except for the stack with the smallest period, where only two bound states (and one resonant state in the GaAs conduction band) exist. The single-particle levels are summarized in Table I. The energetic spacing between the deepest and second-deepest bound state is larger than 90 meV. Consequently, interlevel transitions cannot be mediated by single-phonon scattering (but possibly by multiphonon or polaronic transitions). Along the z-direction, the energy levels are broadened into minibands, with the bandwidth of the lowest miniband ranging from 60 meV for the thinnest spacer layer considered (nominally 13 L of GaAs, or 3.57 nm) to 12 meV for QDs separated by a 21 L (5.82 nm) spacer. Hence the dispersion is sufficiently large to allow for bandlike transport. Within each miniband, scattering of the electrons is possible by low-energy acoustic phonons.

IV. EFFECTIVE-MASS MODEL OF QUANTUM DOT STACKS

In order to efficiently evaluate matrix elements for the electron-phonon scattering, it is convenient to have a simple mathematical model of the electron wave functions at hand. For this purpose, we employ a Kronig-Penney model that offers a good approximative description of the electronic confinement potential of stacks of disk-shaped QDs. A useful approximation is to represent this confinement potential as a sum of two independent potentials $V(\rho,z)\approx V(\rho)+V(z)$, the first one describing in-plane confinement, and the second one describing a periodic sequence of quantum wells in z direction (cf. Ref. 7). This approximation is shown to be adequate for the below-the-barrier states in the conduction band of the QD-superlattices.[38] Using Bloch's theorem, the solution of the Schrödinger equation can now be written in multiplicative form, $\Psi(\rho,z)=R(\rho)u_{k_z}(z)e^{ik_zz}$. The factors are obtained by solving two independent equations,

$$-\frac{\hbar^2}{2m_i^*}\frac{d^2\psi(z)}{dz^2}+V(z)u_{k_z}(z)=\mathcal{E}_n(k_z)u_{k_z}(z), \tag{6}$$

$$-\frac{\hbar^2}{2m_i^*}\left\{\frac{1}{\rho}\frac{d}{d\rho}\left[\rho\frac{dR(\rho)}{d\rho}\right]-\frac{m^2}{\rho^2}R(\rho)\right\}+V(\rho)R(\rho,z)=E_JR(\rho), \tag{7}$$

where m is an integer angular momentum quantum number, $m_i^*=m_1^*$ is the effective mass at the conduction band edge in

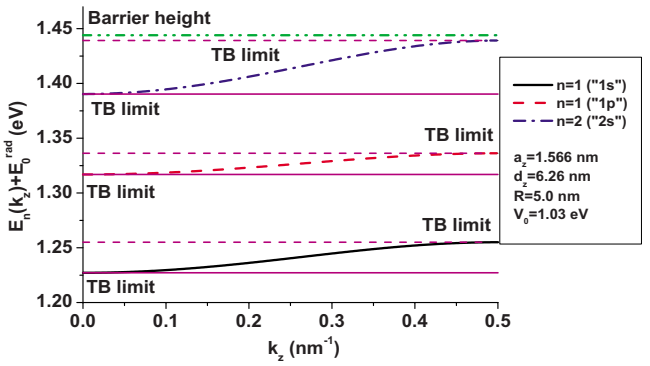

FIG. 1. (Color online) The renormalized minibands in a stack of InAs/GaAs QDs with geometrical parameters indicated in the inset. The valence band top of GaAs is taken as the zero of the energy scale. A dash-dot-dotted (green) line represents the position of the barrier.

the QD and $m_i^*=m_2^*$ is that in the barrier. For an InAs $[m_1^*=0.022m_e$ (Ref. 39)] QD in GaAs $[m_2^*=0.0655m_e$ (Ref. 39)], the interface band offset is estimated to be $V_0=1.030$ eV for the conduction band and $V_{0,\mathrm{vb}}=0.054$ eV for the valence band (in line with Ref. 33). The miniband dispersion in the stack of QDs is obtained as

$$\varepsilon_{J,n}(k_z)=\mathcal{E}_n(k_z)+E_J. \tag{8}$$

The results of the Kronig-Penney model (see, e.g., Ref. 40) are in a qualitative agreement with the band energies obtained from the tight-binding model, though the former can account for the strain effect only via a modification of the model parameters. For the further calculation of the transport coefficients, we renormalize the minibands obtained within the Kronig-Penney model by adjusting the energy values at the center and at the edge of the first Brillouin zone to those obtained using the tight-binding approach. The resulting renormalized bands are shown in Fig. 1.

For the dispersion of the continuum states in the host, we use a parabolic approximation,

$$k=\sqrt{\frac{2\tilde{m}}{\hbar^2}(\varepsilon-V_{0c})}. \tag{9}$$

with a geometry-averaged effective mass $\tilde{m}$ and the conduction band minimum of the GaAs host $V_{0c}=1.444$ eV (measured relative to the valence band maximum).

V. PHONON SCATTERING RATE

Acoustic phonons in the QD stack are treated within the continuum elasticity theory[41] of an effective medium. The velocity of sound is obtained as

$$v_L=\frac{d_z}{\frac{a_z}{v_{\mathrm{InAs}}}+\frac{b_z}{v_{\mathrm{GaAs}}}}. \tag{10}$$

with the sound velocities $v_{\mathrm{InAs}}=3.83$ km/s and $v_{\mathrm{GaAs}}=4.73$ km/s (Ref. 39). To check the validity of the effective medium approach, we additionally calculated the dispersion curves using the Rytov's dispersion relations (p. 73 of Ref. 42). Small deviations of the model of an effective medium from the rigorous results occur only in close vicinity to the center and the boundary of the first Brillouin zone. An explicit calculation of the dispersion relation $\omega(q)$ for acoustic phonons reveals that the effective medium approximation can be applied with a good accuracy. The Hamiltonian of the deformation electron-phonon interaction is

$$H_{e-ph}=ia_c\sum_{\mathbf{q}}\sqrt{\frac{\hbar}{2V\rho\omega(\mathbf{q})}}q(a_{\mathbf{q}}e^{i\mathbf{q}\cdot\mathbf{r}}-a_{\mathbf{q}}^{\dagger}e^{-i\mathbf{q}\cdot\mathbf{r}}), \tag{11}$$

where a_c in the deformation potential, ρ is the mass density and $V=SL$ is the volume of the crystal, S is its cross-sectional area in the xy-plane and $L=Nd_z$ is its height along the z axis. Both the mass density ρ and the deformation potential for the effective medium are calculated as geometry-weighted averages from the quantities of the pure materials, using $\rho_{\mathrm{InAs}}=5.6678\times10^3$ kg/m^3, $\rho_{\mathrm{GaAs}}=5.3175\times10^3$ kg/m^3, $a_{c,\mathrm{InAs}}=-10.2$ eV, and $a_{c,\mathrm{GaAs}}=-11.0$ eV adopted from literature.[39]

We consider intersubband transitions in miniband J assisted by acoustic phonons: $\omega(\mathbf{q})=v_Lq$ with the effective sound velocity given by Eq. (10). The transition probability rate is represented in the form

$$W(J,k_z\to J',k_z')=W^+(J,k_z\to J',k_z')+W^-(J,k_z\to J',k_z').$$

For the phonon occupation factors entering W the high-temperature approximation is used,

$$N_q=\frac{1}{\exp\left(\frac{\hbar v_Lq}{k_BT}\right)-1}\approx\frac{k_BT}{\hbar v_Lq}\approx N_q+1.$$

The detailed calculation of contributions due to the processes with absorption (W^+) and emission (W^-) of a phonon is described in the Appendix.

VI. RELAXATION TIME

The transport properties of the stack of QDs are analyzed using the Boltzmann transport equation.[29,43] Comparing the terms linear in the electric field or the temperature gradient ∇T in the both sides of the Boltzmann transport equation, we get an integral equation with respect to the relaxation time $\tau_i(\varepsilon_\perp',n')$

$$1=\sum_{\mathbf{k}_\perp'k_z'}W(\mathbf{k}_\perp,k_z\to\mathbf{k}_\perp',k_z')\times\left[\tau_i(\varepsilon_\perp,k_z)-\frac{v_i(\mathbf{k}_\perp',k_z')}{v_i(\mathbf{k}_\perp,k_z)}\tau_i(\varepsilon_\perp',k_z')\right]\times\frac{1-f_0(\varepsilon')}{1-f_0(\varepsilon)}. \tag{12}$$

We have shown, that with a high accuracy the dispersion of the relaxation time *in the integrand* can be neglected. In this case one obtains an approximate solution of the Eq. (12):

$$\tau_i^{(1)}(\varepsilon_\perp,n) \approx \left\{ \sum_{\mathbf{k}'n'} W(\mathbf{k},n \to \mathbf{k}',n') \times \left[1 - \frac{v_i(\mathbf{k}',n')}{v_i(\mathbf{k},n)} \right] \frac{1-f_0(\varepsilon')}{1-f_0(\varepsilon)} \right\}^{-1}.$$

We consider further the transport along the z axis in each miniband separately, so that $i=3$ and

$$v_{z,J}(k_z) = \frac{1}{\hbar} \frac{\partial \varepsilon_{J,n}(k_z)}{\partial k_z}. \tag{13}$$

As shown by our numerical calculation, for room temperature the relaxation time can be accurately found from the equation for a nondegenerate semiconductor $[f_0(\varepsilon) \ll 1]$:

$$1 = \sum_{k_z'} W(k_z \to k_z') \left[\tau_{\parallel,J}(k_z) - \frac{v_{z,J}(k_z')}{v_{z,J}(k_z)} \tau_{\parallel,J}(k_z') \right],$$

$$k_z = \frac{\pi}{d} \frac{m}{N}, \quad m = -N/2, \ldots, N/2. \tag{14}$$

In what follows, we use the energy-independent relaxation time for a quantum well of width a_z given by (5) of Ref. 44

$$\tau_{QW} = \frac{2a_z \hbar^3 \rho v_L^2}{3\tilde{m} a_c^2 k_B T} \tag{15}$$

to define a dimensionless quantity for each miniband J:

$$\tau_{\parallel,J}(k_z) = \tilde{\tau}_{\parallel,J}(k_z) \tau_{QW}.$$

The resulting integral equation, after inserting Eqs. (A2) and (A3) and summation over q_z, is

$$1 = \frac{1}{2\pi} \frac{a}{3\tilde{m} v_L^2} \int_{-\pi/d_z}^{\pi/d_z} dk_z' \sum_{n=-\infty}^{\infty} |C_n(k_z',k_z)|^2 \times \{ |M_{JJ}(q_{\perp 0}^+(k_z' - k_z + 2\pi n/d_z))|^2 |\varepsilon_{k_z'} - \varepsilon_{k_z}| \Theta(\varepsilon_{k_z'} - \varepsilon_{k_z}) \Theta((q_{\perp 0}^+)^2) + |M_{JJ}(q_{\perp 0}^-(k_z' - k_z + 2\pi n/d_z))|^2 |\varepsilon_{k_z'} - \varepsilon_{k_z}| \Theta(-\varepsilon_{k_z'} + \varepsilon_{k_z}) \Theta((q_{\perp 0}^-)^2) \} \times \left[\tilde{\tau}_{\parallel,J}(k_z) - \frac{v_z(k_z')}{v_z(k_z)} \tilde{\tau}_{\parallel,J}(k_z') \right], \tag{16}$$

where $\Theta(\varepsilon)$ is a Heaviside step function.

The relaxation time for three minibands in a QD stack resulting from the numerical solution of the integral Eq. (16) is plotted in Fig. 2, revealing a strong variation as a function of k_z. It behaves similarly for the first and second minibands, being somewhat larger for the second. The third miniband, formed from states with a much weaker confinement than that for the first and second minibands, shows a larger band dispersion and a much larger relaxation time. The very pronounced structure as a function of k_z is due to the interplay between the conditions of the non-vanishing contributions of the phonon-assisted processes to the probability rate from Eq. (A5) and (A8). By the same reasons the relaxation time for the first two minibands shows small kinks in the range from 0.1 to 0.4 nm^{-1}. A widely used approximation of a constant relaxation time is not adequate for a stack for semiconductor QDs. The rise of the relaxation time toward the boundaries of the Brillouin zone, as seen in Fig. 2, is a common feature for all QD geometries investigated.

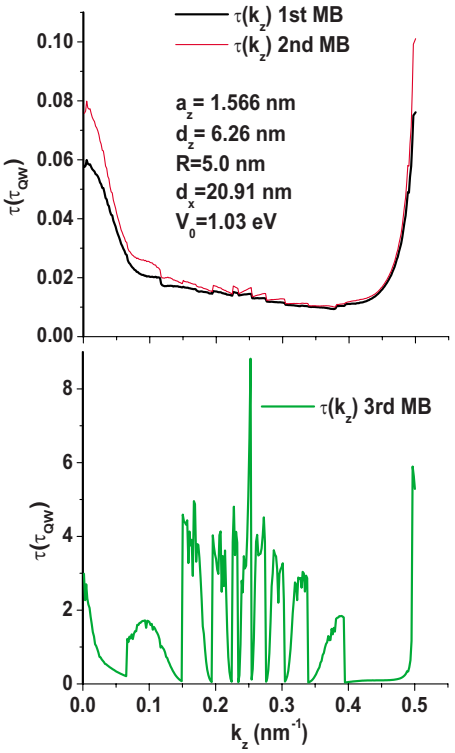

FIG. 2. (Color online) The relaxation time for two minibands in a stack of InAs/GaAs QDs with geometrical parameters indicated in the inset. τ_{QW} is a constant relaxation time for a quantum well of width a_z of Ref. 44.

For the states in the continuum of the host material, scattering by acoustic phonons is less critical. In this case, an approximative solution of the Eq. (12) can be obtained by neglecting the dispersion of the relaxation time in the integrand,

$$\frac{1}{\tau_i^{(1)}(\varepsilon)} \approx \sum_{\mathbf{k}'} W(\mathbf{k} \to \mathbf{k}') \left[1 - \frac{v_i(\mathbf{k}')}{v_i(\mathbf{k})} \right] \frac{1-f_0(\varepsilon')}{1-f_0(\varepsilon)}. \tag{17}$$

We consider further the transport along the z axis, so that $i=3$ and

$$v_z(\mathbf{k}) = \frac{1}{\hbar} \frac{\partial \varepsilon(\mathbf{k})}{\partial k_z} = \frac{\hbar k_z}{\tilde{m}}.$$

The relaxation time given by Eq. (17) in a nondegenerate semiconductor $[f_0(\varepsilon,n) \ll 1]$ acquires the form:

$$\frac{1}{\tau_\parallel^{(1)}(\varepsilon)} \approx \sum_{\mathbf{k}'} W(\mathbf{k} \to \mathbf{k}') \left[1 - \frac{k_z'}{k_z} \right]. \tag{18}$$

Following,[43] we find

$$\tau_\parallel^{(1)}(\varepsilon) \approx \frac{\pi \rho \hbar^4 v_L^2}{\sqrt{2} \tilde{m}^{3/2} a_c^2 k_B T} \frac{1}{\sqrt{\varepsilon - V_{0c}}}. \tag{19}$$

VII. DOPING

While nanostructuring enables one to tailor a material with a highly structured density of states (DOS), population of these states by doping is crucial to obtain good thermoelectric performance. The amount of charge carriers introduced by doping determines where the chemical potential is located within the highly structured DOS. For the InAs/GaAs system, we consider n-type doping with a concentration n_D of donor impurities possessing the charge transfer energy level ε_D. The position of the chemical potential μ is determined implicitly by the condition of neutrality in the form

$$n + n_D' = n_D. \tag{20}$$

In our model comprising both minibands and continuum states, the total conduction electron density n is the sum of both contributions,

$$n(\mu) = \sum_{J,n} \frac{2}{\pi \mathcal{A}} \int_0^{\pi/d_z} dk_z f_0(\varepsilon_{J,n}(k_z)) + \frac{\sqrt{2}\tilde{m}^{3/2}}{\pi^2 \hbar^3} \int_{V_{0c}}^{\infty} \sqrt{\varepsilon - V_{0c}} f_0(\varepsilon) d\varepsilon,$$

where the dependence on μ enters via the Fermi distribution function f_0. n_D' is the concentration of electrons occupying donor levels. In equilibrium, it can be represented as [cf. Eq. (28.32) of Ref. 29]

$$n_D'(\mu) = \frac{n_D}{\frac{1}{g}\exp\left(\frac{\varepsilon_D - \mu}{k_B T}\right) + 1}, \tag{21}$$

where $g=2$ is the degeneracy factor for the donor state. Substituting Eq. (21) into Eq. (20), we find the electroneutrality condition in the form

$$n(\mu) = n_D \frac{1}{g \exp\left(\frac{\mu - \varepsilon_D}{k_B T}\right) + 1}. \tag{22}$$

The relation between n and n_D is evaluated numerically, assuming shallow donors, i.e., $\varepsilon_D = 1.434$ eV close to the conduction band minimum $V_{0c} = 1.444$ eV. By monitoring separately the occupation of each miniband, we show that, for experimentally relevant donor concentrations, the number of electrons in a QD is less than or of the order of unity. This ensures that the on-site repulsion of electrons in the same QD can be safely neglected.

VIII. RESULTS

As shown previously,[46] the electric conductivities for minibands, calculated according to Eq. (2), reveal peaks at such values of the chemical potential μ (and, correspondingly, of the donor concentration), where μ lies inside a miniband. With increasing temperature, those peaks get smaller and broader.

Here, we present results as a function of the doping concentration, using a model that includes both the minibands and the continuum of the host conduction band. Therefore, miniband features in the conductivity are noticeable only in certain ranges of doping and temperature. For example, for a stack with $a_z = 1.566$ nm and $d_z = 6.26$ nm, only one peak at $n_D \approx 1.5 \times 10^{25}$ m^{-3} persists in the presence of a continuum [Fig. 3(a)], which is mainly due to the third miniband. This peak visible at $T = 100$ K sits at the foot of the continuum-determined increase which dominates at higher doping concentrations. The peak in σ is significantly reduced when the temperature increases up to 200 K, and disappears when the temperature further rises up to 300 K. The behavior of the electron heat conductivity κ_e obtained from Eq. (4) is qualitatively similar to the electric conductivity [see Fig. 3(b)]. The peak in κ_e due to the minibands has its maximum at $n_D \approx 5 \times 10^{25}$ m^{-3}, i.e., at somewhat higher doping concentrations, and is significantly broader than a peak of the electric conductivity. The continuum-determined rise in the electron heat conductivity dominates its behavior with increasing donor concentration.

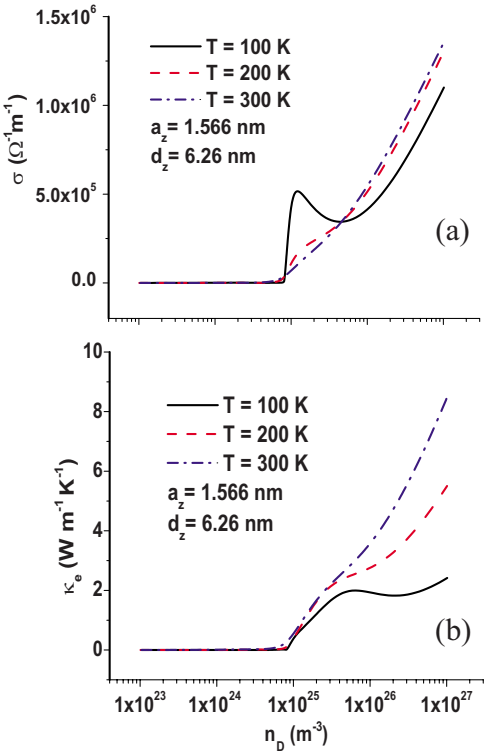

FIG. 3. (Color online) The electric conductivity (a) and the electron heat conductivity (b) in a stack of InAs/GaAs QDs taking into account a continuum of states.

Next, we discuss the Seebeck coefficient obtained from Eq. (3). At low temperatures ($T = 100$ K), it changes sign four times: The first zero of S at $n_D \approx 2 \times 10^{24}$ m^{-3} occurs when the Fermi energy reaches the center of the first miniband. The second zero of S at $n_D \approx 3 \times 10^{24}$ m^{-3} corresponds to the Fermi level lying in between the first and the second minibands: In this case, both minibands are partially occupied and thus contribute to the transport, but the "holes" in the first miniband and the electrons in the second miniband contribute to S with opposite sign. When the Fermi energy reaches the center of the second miniband, one might expect

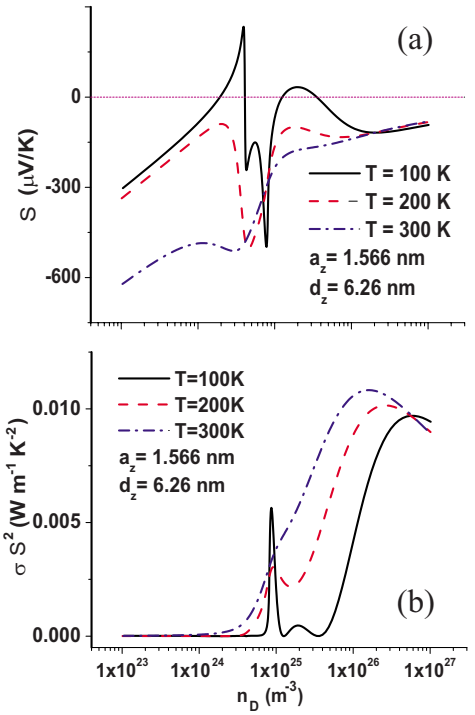

FIG. 4. (Color online) The Seebeck coefficient (a) and the power factor (b) in a stack of InAs/GaAs QDs taking into account a continuum of states.

another zero of the Seebeck coefficient, but the situation is more complex due to the closeness of the third miniband and the continuum: After a minimum of S at $n_D \approx 4 \times 10^{24}$ m^{-3}, a maximum of S emerges at $n_D \approx 5 \times 10^{24}$ m^{-3}. A deep minimum of S at $n_D \approx 0.8 \times 10^{25}$ m^{-3} corresponds to the Fermi level reaching the bottom of the third miniband. The third zero at $n_D \approx 1.5 \times 10^{25}$ m^{-3} occurs when the Fermi energy reaches the center of the third miniband: just at this value of the concentration the electric conductivity has it maximum [see Fig. 3(a)]. The fourth zero of S at $n_D \approx 4 \times 10^{25}$ m^{-3} reflects the emerging dominance of continuum states. At higher temperatures, the miniband structure in S is progressively shifted to lower concentrations (away from a continuum) and washed out. At $T=200$ and 300 K, S reveals only one minimum at $n_D \approx 4 \times 10^{24}$ m^{-3} and a very shallow minimum at $n_D \approx 3 \times 10^{24}$ m^{-3}, respectively. At 300 K and above, all minibands remain less than half-filled. In this situation, S is negative and displays a linear increase over some ranges of doping concentration, a behavior known from n-doped bulk semiconductors. However, the effects of nanostructuring on the band structure are strong enough to result in notable features in S at lower temperatures ($T \lesssim 200$ K). Consequently, at $T=100$ K the power factor [Fig. 4(b)] reveals a structure with two peaks at $n_D \approx 0.8 \times 10^{25}$ m^{-3} and $n_D \approx 2 \times 10^{25}$ m^{-3} due to minibands and a broad common peak due to continuum states with a maximum at much higher concentrations, $n_D \approx 5 \times 10^{26}$ m^{-3}. It is noteworthy that the first prominent peak due to the miniband is of comparable height with the peak due to the continuum. The analyzed features of the power factor translate into similar structures in the figure-of-merit, as discussed below. With increasing temperature up to $T=200$ K and then to T

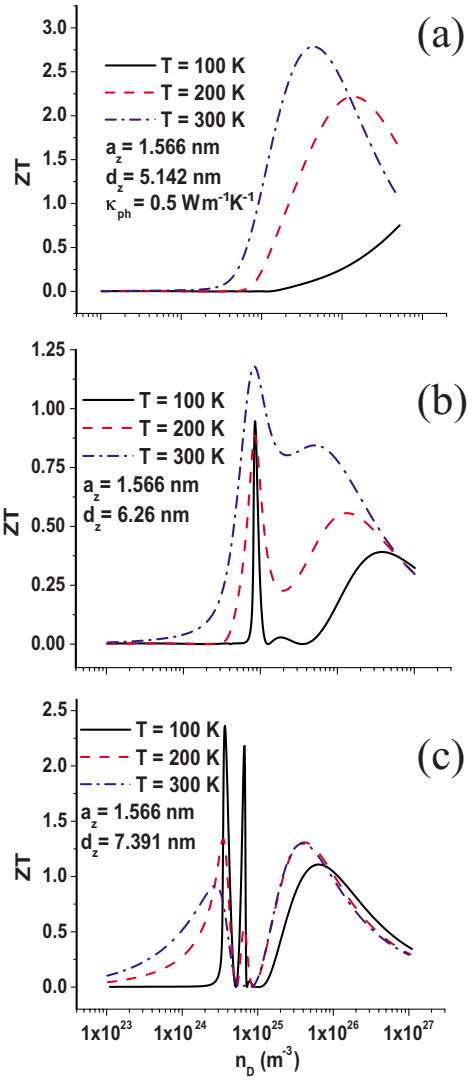

FIG. 5. (Color online) The figure-of-merit for stacks of InAs/GaAs QDs with $a_z=1.566$ nm, (a) $d_z=5.142$ nm, (b) $d_z=6.26$ nm, and (c) $d_z=7.391$ nm including an estimate for the phonon heat conductivity.

$=300$ K the first peak starts to broaden and then develops into a shoulder on the larger, continuum-determined peak.

Previously, we showed that our model of the QD stack yields very high values of the figure-of-merit if the phonon contribution to the thermal conductivity is disregarded.[46] From the literature, one finds that the overall thermal conductivity of QD stacks may well be below 1 W/(m K) (Ref. 14), and even values of the phonon heat conductivity as low as $\kappa_{ph} \approx 0.1$ W/(m K) are theoretically predicted for nanowires (Ref. 45). Tentatively, we use $\kappa_{ph}=0.5$ W/(m K) in addition to κ_{el} in the following estimates. Then κ_{ph} dominates over κ_{el} [as calculated from Eq. (4)] as long as $n_D \lesssim 1 \times 10^{25}$ m^{-3}, cf. Figure 3(b). The figure-of-merit ZT as a function of the donor concentration obtained from Eq. (5) is plotted in Figs. 5(a)–5(c). For a short-period stack (with $d_z=5.142$ nm), ZT displays a broad maximum as a function of n_D; on this background the contributions from the minibands are hidden. With increasing n_D, the increase in the number of electronic carriers in the host conduction band is responsible

for the initial rise of ZT. For high temperatures and very high values of n_D, ZT drops again due to the electronic contribution to the thermal conductivity rising more steeply than the electrical conductivity at $T=300$ K, cf. Figure 3. This results in the continuum-determined peak, e.g., seen at $n_D \approx 3 \times 10^{25}$ m^{-3} for $T=300$ K in Fig. 5(a). For stacks with a larger period (with $d_z=6.26$ nm and $d_z=7.391$ nm), our calculation reveals certain windows of enhanced thermoelectric efficiency due to the minibands, where the figure-of-merit achieves the values ~ 1 (at $n_D \approx 1 \times 10^{25}$ m^{-3}) for $d_z=6.26$ nm and ~ 2 (at $n_D \approx 4 \times 10^{24}$ m^{-3} and $n_D \approx 6 \times 10^{24}$ m^{-3}) for $d_z=7.391$ nm. These optimum values of the donor concentration are a function of geometrical parameters of the QD stack. With rising temperature, the above features of the figure-of-merit are broadened. However, the peaks due to the first miniband remain prominent up to $T=300$ K.

For taller QDs that support more deeply bound states and a larger number of minibands, the contributions of the highest miniband and of the continuum to the figure-of-merit merge into a single peak (Fig. 6). When increasing the height of the QD to $a_z=2.193$ nm [Fig. 6(a) and 6(b)] and to $a_z=2.8185$ nm [Fig. 6(c)], the peak structure due to the lowest miniband is visible only at low temperature ($T=100$ K), and is small compared to the continuum peak. At higher temperature, the effect of the minibands shows up as a shoulder of the continuum peak, leading to a sharp rise of ZT around $n_D \approx 10^{25}$ m^{-3}.

In summary, we expect an advantage in the figure-of-merit for QD stacks over bulk material in an intermediate regime where the minibands contribute significantly to the electric conductivity, while the corresponding contribution of the electrons to the heat conduction is still low. For the studied sample geometries, this regime corresponds to a doping concentration of $n_D \lesssim 10^{25}$ m^{-3}. Assuming a sufficiently low lattice contribution to the thermal conductivity, ZT values in excess of unity can be reached. For a given height of the QDs of less than 2 nm, the figure-of-merit shows sharp peaks at specific values of n_D if the QDs are separated by a spacer layer of about 5 nm or more, whereas the miniband features remain hidden for thinner spacer layers or taller QDs. In the latter case, the effect of nanostructuring shows up as an enhancement of ZT right at the onset of the host conduction band (corresponding to $n_D \approx 1.5 \times 10^{25}$ m^{-3} in the present case). Comparing samples with the same stacking period of 7.4 nm [Figs. 6(b) and 6(c)], we find that this enhancement yields a ZT value of about 2.7 at room temperature, and is rather insensitive to QD height.

IX. CONCLUSION

An approach has been elaborated for numerical calculation of the electron dispersion, the transport relaxation time and the transport coefficients in a 1D stack of disk-shaped InAs/GaAs QDs. By calculating the relaxation time for acoustic-phonon scattering explicitly, we show that the popular approximation of a constant relaxation time is not adequate for cross-plane transport through a stack for semiconductor QDs. From the numerical analysis of the electric and thermal conductivities, the Seebeck coefficient and the

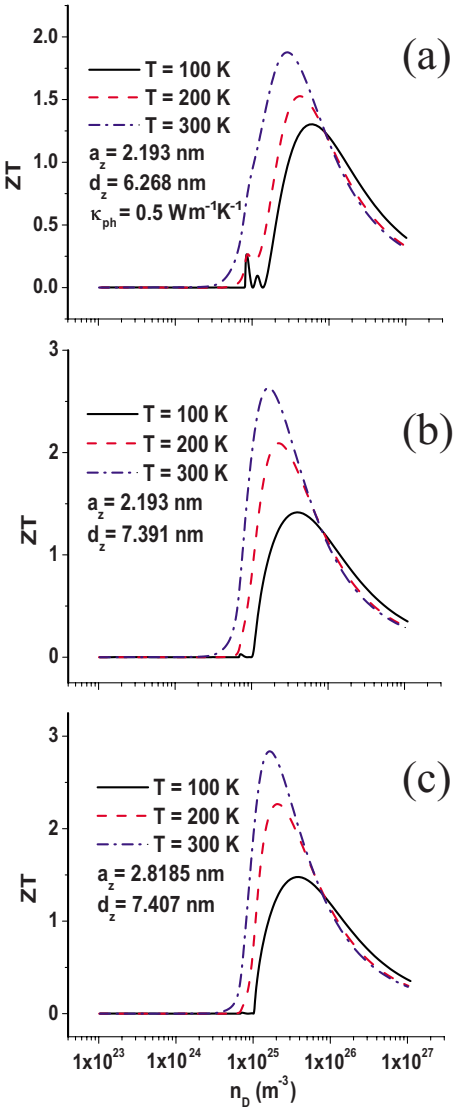

FIG. 6. (Color online) The figure-of-merit for stacks of InAs/GaAs QDs with (a) $a_z=2.193$ nm, $d_z=6.268$ nm, (b) $a_z=2.193$ nm, $d_z=7.399$ nm, and (c) $a_z=2.8185$ nm, $d_z=7.407$ nm including an estimate for the phonon heat conductivity.

figure-of-merit, we conclude that electronic signatures of nanostructuring should be detectable in the thermoelectric response of a 1D stack of QDs. For judiciously chosen values of the donor concentration, depending on the geometrical parameters of the QD superlattice, the thermoelectric power factor is strongly enhanced. Hence a QD superlattice exemplifies a materials system whose efficiency as a thermoelectric converter is controlled by its geometry on the nanoscale. The thermoelectric figure-of-merit as a function of the donor concentration reflects the miniband electron energy spectrum of the QD stack, and thus can be used as an experimental fingerprint of its electronic structure. This method should work best for low temperatures and flat QDs. The highest values of ZT are reached for QDs separated by very thin spacer layers, when the miniband features in transport merge with the background due to the conduction band of the host material. For the material system studied, InAs QDs in GaAs, the predicted figure-of-merit achieves, at optimal ar-

chitecture of the stack, maximal values of ~2.7, assuming values of the phonon heat conductivity $\kappa_{ph} \sim 0.5$ W/(m K), i.e., close to those presently reported. Our results imply that for technical exploitation of QD superlattices as thermoelectric converters choosing the optimal architecture and doping concentration is of paramount importance.

ACKNOWLEDGMENTS

We acknowledge fruitful collaboration with O. G. Schmidt and A. Rastelli and useful discussions with G. Chen, S. L. Chuang, E. A. Hoffmann, H. Linke, J. E. Matthews, A. Shakouri, and Y. Zhang. A. Kleinsorge and T. Hammerschmidt are thanked for developing and providing codes for atomistic modeling. The financial support from the German Research Foundation (DFG) under Grant No. SPP 1386 is acknowledged. V.M.F. is grateful to the Faculty of Physics for support during his stay at the University of Duisburg-Essen, the European Science Foundation (ESF) for the Exchange Grant No. 2157 within the activity 'Arrays of Quantum Dots and Josephson Junctions' and the German Academic Exchange Service (DAAD).

APPENDIX: EVALUATION OF THE SCATTERING RATE FOR THE ACOUSTIC PHONON SCATTERING WITHIN A MINIBAND

The basis wave functions

$$|J,k_z,N_{\mathbf{q}}\rangle = \Psi_J(\rho)\frac{e^{ik_z z}}{\sqrt{N}}u_{k_z}(z)|N_{\mathbf{q}}\rangle \tag{A1}$$

are characterized by the quantum number J of the transverse motion, the wave vector k_z, the Bloch function $u_{k_z}(z)$ and the occupation number of phonons $N_{\mathbf{q}}$. The contributions due to the processes with absorption (W^+) and emission (W^-) of a phonon are as follows:

$$W^+(k_z \to k_z') = \frac{1}{2\pi}\int q_\perp dq_\perp \sum_{q_z} \frac{\pi a_c^2 kT}{L\rho\hbar v_L^2}|M_{JJ}(q_\perp)|^2 \delta(\varepsilon_{k_z'} - \varepsilon_{k_z} - \hbar v_L\sqrt{q_\perp^2 + q_z^2}) \times \sum_{n=-\infty}^{\infty} |C_n(k_z',k_z)|^2 \delta_{k_z',k_z+q_z-2\pi n/d_z}, \tag{A2}$$

$$W^-(k_z \to k_z') = \frac{1}{2\pi}\int q_\perp dq_\perp \sum_{q_z} \frac{\pi a_c^2 kT}{L\rho\hbar v_L^2}|M_{JJ}(q_\perp)|^2 \delta(\varepsilon_{k_z'} - \varepsilon_{k_z} + \hbar v_L\sqrt{q_\perp^2 + q_z^2}) \times \sum_{n=-\infty}^{\infty} |C_n(k_z',k_z)|^2 \delta_{k_z',k_z-q_z-2\pi n/d_z}. \tag{A3}$$

Here the overlap integral for the in-plane motion is

$$M_{J'J}(\mathbf{q}_\perp) = \int d^2\rho \Psi_{J'}^*(\rho) e^{i\mathbf{q}_\perp\cdot\rho}\Psi_J(\rho), \quad q = \sqrt{q_\perp^2 + q_z^2},$$

while the overlap integral of the Bloch functions is

$$C_n(k_z',k_z) = \int_{-b_z}^{a_z} dz' \exp\left(-i\frac{2\pi n}{d_z}z'\right) u_{k_z'}^*(z') u_{k_z}(z').$$

The sum over n in Eqs. (A2) and (A3) reflects the "Floquet sidebands" owing to the periodicity of the Bloch functions with a period d_z:

$$u_{k_z'}^*(z)u_{k_z}(z) = \sum_{n=-\infty}^{\infty} \exp\left(i\frac{2\pi n}{d_z}z\right)\frac{1}{d_z}C_n(k_z',k_z). \tag{A4}$$

The integrations over $q_\perp$ Eqs. (A2) and (A3) are performed analytically. The nonvanishing contributions to the integral over $q_\perp$ occur when two conditions are satisfied for W^+:

$$\varepsilon_{k_z'} - \varepsilon_{k_z} \geq 0; \tag{A5}$$

$$(q_{\perp 0}^+(q_z))^2 \equiv \left(\frac{\varepsilon_{k_z'} - \varepsilon_{k_z}}{\hbar v_L}\right)^2 - q_z^2 \geq 0 \tag{A6}$$

and two conditions for W^-:

$$\varepsilon_{k_z'} - \varepsilon_{k_z} \leq 0; \tag{A7}$$

$$(q_{\perp 0}^-(q_z))^2 \equiv \left(\frac{\varepsilon_{k_z'} - \varepsilon_{k_z}}{\hbar v_L}\right)^2 - q_z^2 \geq 0. \tag{A8}$$

These conditions reflect the conservation of energy in the course of the phonon-assisted transitions.

*v.fomin@ifw-dresden.de
†peter.kratzer@uni-due.de

[1] L. D. Hicks, T. C. Harman, and M. S. Dresselhaus, Appl. Phys. Lett. **63**, 3230 (1993).
[2] T. E. Humphrey and H. Linke, Phys. Rev. Lett. **94**, 096601 (2005).
[3] G. D. Mahan and J. O. Sofo, Proc. Natl. Acad. Sci. USA **93**, 7436 (1996).
[4] X. Zianni, Phys. Rev. B **78**, 165327 (2008).
[5] S. J. Thiagarajan, V. Jovovic, and J. P. Heremans, Phys. Status Solidi (RRL) **1**, 256 (2007).
[6] Y.-M. Lin and M. S. Dresselhaus, Phys. Rev. B **68**, 075304 (2003).
[7] O. L. Lazarenkova and A. A. Balandin, Phys. Rev. B **66**, 245319 (2002).
[8] A. A. Balandin and O. L. Lazarenkova, Appl. Phys. Lett. **82**, 415 (2003).
[9] T. C. Harman, P. J. Taylor, M. P. Walsh, and B. E. LaForge, Science **297**, 2229 (2002).
[10] Y. K. Koh, C. J. Vineis, S. D. Calawa, M. P. Walsh, and D. G. Cahill, Appl. Phys. Lett. **94**, 153101 (2009).
[11] M. S. Dresselhaus, G. Chen, M. Y. Tang, R. Yang, H. Lee, D.

Wang, Z. Ren, J.-P. Fleurial, and P. Gogna, Adv. Mater. **19**, 1043 (2007).
[12] Y. Ma, Q. Hao, B. Poudel, Y. Lan, B. Yu, D. Wang, G. Chen, and Z. Ren, Nano Lett. **8**, 2580 (2008).
[13] G. Joshi, H. Lee, Y. Lan, X. Wang, G. Zhu, D. Wang, R. W. Gould, D. C. Cuff, M. Y. Tang, M. S. Dresselhaus, G. Chen, and Z. Ren, Nano Lett. **8**, 4670 (2008).
[14] G. Pernot, M. Stoffel, I. Savic, F. Pezzoli, P. Chen, G. Savelli, A. Jacquot, J. Schumann, U. Denker, I. Mönch, Ch. Deneke, O. G. Schmidt, J. M. Rampnoux, S. Wang, M. Plissonnier, A. Rastelli, S. Dilhaire, and N. Mingo, Nature Mater. **9**, 491 (2010).
[15] J. Cai and G. D. Mahan, Phys. Rev. B **78**, 035115 (2008).
[16] A. Yadav, K. P. Pipe, W. Ye, and R. S. Goldman, J. Appl. Phys. **105**, 093711 (2009).
[17] S. V. Faleev and F. Leonard, Phys. Rev. B **77**, 214304 (2008).
[18] M. Zebarjadi, K. Esfarjani, A. Shakouri, J.-H. Bahk, and Z. Bian, Appl. Phys. Lett. **94**, 202105 (2009).
[19] R. Scheibner, E. G. Novik, T. Borzenko, M. Konig, D. Reuter, A. D. Wieck, H. Buhmann, and L. W. Molenkamp, Phys. Rev. B **75**, 041301 (2007).
[20] E. A. Hoffmann, N. Nakpathomkun, A. I. Persson, H. Linke, H. A. Nilsson, and L. Samuelson, Appl. Phys. Lett. **91**, 252114 (2007).
[21] E. A. Hoffmann, N. Nakpathomkun, A. I. Persson, H. A. Nilsson, L. Samuelson, and H. Linke, Physica E (Amsterdam) **40**, 1605 (2008).
[22] T. P. Martin, M. S. Fairbanks, B. C. Scannell, C. A. Marlow, H. Linke, and R. P. Taylor, Appl. Phys. Lett. **95**, 182105 (2009).
[23] P. Mani, N. Nakpathomkun, and H. Linke, J. Electron. Mater. **38**, 1163 (2009).
[24] D. Bimberg, M. Grundmann, and N. N. Ledentsov, *Quantum Dot Heterostructures* (Wiley, Chichester, 1999).
[25] Z. M. Wang, K. Holmes, Y. I. Mazur, and G. J. Salamo, Appl. Phys. Lett. **84**, 1931 (2004).
[26] L. Li, D. Guimard, M. Rajesh, and Y. Arakawa, Appl. Phys. Lett. **92**, 263105 (2008).
[27] D. Grützmacher, T. Fromherz, C. Dais, J. Stangl, E. Müller, Y. Ekinci, H. H. Solak, H. Sigg, R. T. Lechner, E. Wintersberger, S. Birner, V. Holý, and G. Bauer, Nano Lett. **7**, 3150 (2007).
[28] S. Kiravittaya, A. Rastelli, and O. G. Schmidt, Rep. Prog. Phys. **72**, 046502 (2009).
[29] N. W. Ashcroft and N. D. Mermin, *Solid State Physics* (Saunders College, Philadelphia, 1976).
[30] G. S. Nolas, J. Sharp, and H. J. Goldsmid, *Thermoelectrics* (Springer, Berlin, 2001).
[31] T. Hammerschmidt, P. Kratzer, and M. Scheffler, Phys. Rev. B **77**, 235303 (2008); **81**, 159905(E) (2010).
[32] T. B. Boykin, Phys. Rev. B **56**, 9613 (1997).
[33] L.-W. Wang, J. Kim, and A. Zunger, Phys. Rev. B **59**, 5678 (1999).
[34] R. Santoprete, B. Koiller, R. B. Capaz, P. Kratzer, Q. K. K. Liu, and M. Scheffler, Phys. Rev. B **68**, 235311 (2003).
[35] R. Santoprete, P. Kratzer, M. Scheffler, R. B. Capaz, and B. Koiller, J. Appl. Phys. **102**, 023711 (2007).
[36] R. B. Capaz, G. C. de Araujo, B. Koiller, and J. P. von der Weid, J. Appl. Phys. **74**, 5531 (1993).
[37] L.-W. Wang and A. Zunger, J. Chem. Phys. **100**, 2394 (1994).
[38] D. L. Nika, E. P. Pokatilov, Q. Shao, and A. A. Balandin, Phys. Rev. B **76**, 125417 (2007).
[39] *Handbook on Physical Properties of Semiconductors*, III-V Compound Semiconductors Vol. 2, edited by S. Adachi (Kluwer, Boston, 2004).
[40] P. Y. Yu and M. Cardona, *Fundamentals of Semiconductors. Physics and Materials Properties* (Springer, Berlin, 1999).
[41] B. A. Auld, *Acoustic Fields and Waves in Solids* (Wiley, New York, 1973), Vol. 1.
[42] S. M. Rytov, Akust. Zh. **2**, 71 (1956) [Sov. Phys. Acoust. **2**, 67 (1956)].
[43] A. I. Anselm, *Introduction to Semiconductor Theory* (Mir, Moscow, 1981); *Introduction to Semiconductor Theory* (Prentice-Hall, Englewood Cliffs, NJ, 1981) (English translation).
[44] S. I. Borisenko, Semiconductors **36**, 1145 (2002).
[45] N. Mingo, Appl. Phys. Lett. **84**, 2652 (2004).
[46] V. M. Fomin and P. Kratzer, Physica E (Amsterdam) **42**, 906 (2010).